



Hydrogen evolution reaction efficiency of carbon nanohorn incorporating molybdenum sulfide and polydopamine/palladium nanoparticles

Balamurugan Devadas^a, Chia Chi Chang^a, Toyoko Imae^{a,b,*}

^a Graduate Institute of Applied Science and Technology, National Taiwan University of Science and Technology, 43 Section 4, Keelung Road, Taipei 10607, Taiwan

^b Department of Chemical Engineering, National Taiwan University of Science and Technology, 43 Section 4, Keelung Road, Taipei 10607, Taiwan

ARTICLE INFO

Article history:

Received 6 August 2018

Revised 30 April 2019

Accepted 17 May 2019

Available online 14 June 2019

Keywords:

Carbon nanohorn

Palladium nanoparticle

Polydopamine

Molybdenum sulfide

Nanocomposite

Hydrogen evolution reaction

ABSTRACT

The involvement of carbon nanohorn (CNH) in molybdenum sulfide (MoS₂) and polydopamine (PDA)/palladium nanoparticles (Pd NPs) was studied for the hydrogen evolution reaction (HER) efficiency. In this research, the in-situ hydrothermal and PDA-assisted chemical reaction routes were adopted to synthesize MoS₂/CNH and PDA-Pd/CNH nanocomposites. The electrochemical studies confirmed the HER activity of PDA-Pd/CNH-modified electrode superior to that of MoS₂/CNH-modified electrode. The coating thickness of PDA was optimized towards high HER efficiency. The enhancement of HER cathodic current density was due to the strong interaction between CNH and Pd NPs. The thin coating by PDA on Pd/CNH nanocomposites maintained the excellent stability and the durability during the HER. Thus, CNH is one of the hopeful carbon materials to enhance the cathodic current density for HER.

© 2019 Taiwan Institute of Chemical Engineers. Published by Elsevier B.V. All rights reserved.

1. Introduction

Strategy of eco-friendly energy resource will maintain the green-world aspect forever. Accordingly, using hydrogen as green energy has major influence on the environment and human health in the world and opens up an additional advancement in new energy world [1,2]. Hence, the existing keen challenge is the hydrogen production via electrochemical water splitting instead of steam reforming process to avoid the CO₂ emission [3]. As a result, the different types of electrocatalysts have been used in water splitting for hydrogen evolution [4,5]. The catalyst consisting of platinum (Pt) is widely known to be a primary material to produce hydrogen at zero overpotential with rapid kinetics [6]. Nonetheless, such noble metal-based catalyst is hitherto known to be unfavorable owing to its costly price [7]. Hence, the motivation of leading researches is to replace Pt-based catalyst for the hydrogen evolution reaction (HER) [8].

On the other hand, carbon-based materials are valid to progress the catalytic activity of component due to their large surface area, stability and durability [9–11]. In particular, they have

hitherto been exploited in many applications such as biomedicine [12–14], energy storage and conversion [15–17], biosensor [18,19] and electrocatalysis [20,21]. Currently, graphene [22] and carbon nanotube (CNT) [23] have great attention as the most efficient support material in the field of HER [24] owing to their excellent durability. In the place of graphene and CNT, the use of other carbon material like carbon nanohorn (CNH) is also noteworthy to evaluate the HER efficiency.

The CNH is the carbon material with horn-shaped units consisting of the sp²-bonded carbon atoms [25]. In general, the CNH has been considered as an alternative attractive material to graphene and CNT due to its excellent unique properties such as wide surface area, effective electric conductivity, large pore volume and distinguished thermal stability [26,27]. Moreover, the internal nanospaces of CNH, which increase the surface to allow the active deposition of small molecules and ions, make CNH to act as a conducting support [26]. Thus, CNH-based nanocomposites have received great attention in multiple applications including electrochemical sensors [28], electrochemical immunosensors [29], oxygen reduction reaction [30] and fuel cells [26]. Our recent reports on CNH indicate that CNH has shown potential for use in energy storage applications [6,31]. Evidently, it is not a surprise that an electrocatalyst of CNH composite including 1 wt% Pt exhibited the excellent electrocatalytic activity towards HER [6].

* Corresponding author at: Graduate Institute of Applied Science and Technology, National Taiwan University of Science and Technology, 43 Section 4, Keelung Road, Taipei 10607, Taiwan.

E-mail address: imae@mail.ntust.edu.tw (T. Imae).

On the other hand, molybdenum sulfide (MoS_2) is a kind of heterogeneous catalysts and may raise Pt-like activity toward HER [32,33]. Though bulk MoS_2 displayed a poor activity to HER [34,35], their sulfur edge sites have extremely encouraged the HER efficiency [36]. Nonetheless, combining carbon and MoS_2 in a controlled manner, the functionality of the MoS_2 can be considerably enhanced [37]. Evidently, there are a few literatures for enhanced HER electrocatalytic activity using MoS_2 /carbon composites [38,39]. In addition, the noble metal nanoparticles possess high purity and electrochemical activities. Among them, palladium (Pd) is often of interest due to its catalytic activities in electrochemical reaction and its cheaper price than Pt [40]. Moreover, the electrocatalytic activity of Pd nanoparticles (Pd NPs) was considerably enhanced by the support of carbon material such as graphene [41]. To the knowledge, there is no report using CNH on composites of MoS_2 and Pd NPs towards HER. Therefore, in this work, the HER efficiency of CNH on both MoS_2 and Pd NPs has been investigated.

In this investigation, the sulphur-enriched MoS_2 and MoS_2 /CNH composite were synthesised via the in-situ hydrothermal route. In addition, PDA-stabilized composite of CNH with Pd NPs (PDA-Pd/CNH) was synthesised through the chemical route. The amount of PDA was controlled towards the high HER efficiency. The enhancement was evaluated by the cathodic current density of the HER. Thus, the efficiency of CNH to enhance the HER activity was discussed and compared between two composites.

2. Experimental section

2.1. Materials

Dopamine hydrochloride (DA, 99%) and ammonium molybdate tetrahydrate ($(\text{NH}_4)_6\text{Mo}_7\text{O}_{24}\cdot 4\text{H}_2\text{O}$) were obtained from Alfa Aesar, England. Palladium(II) chloride (PdCl_2) (59%), thioacetamide ($\text{C}_2\text{H}_5\text{NS}$) and sodium borohydride (NaBH_4) (98%) were purchased from Acros organics, Belgium. CNH was obtained from NEC Corporation, Japan. Other chemicals were the commercial grade and all chemicals were used as received. Aqueous solutions were prepared by using distilled water.

2.2. Synthesis of acid-treated CNH, MoS_2 /CNH, PDA-Pd(0) and PDA-Pd/CNH

For the acidification of CNH, the pristine CNH was oxidized using acid treatment. Pristine CNH (50 mg) was mixed with HNO_3 (30 ml) under the constant stirring, and the mixture was refluxed at 100 °C for 60 min. Then the mixture was cooled down to room temperature, filtered using a membrane filter paper (PTFE, 0.2 μm) and washed with water until the filtrate solution become neutral. Then the acid-treated CNH was dried at 50 °C for overnight.

The synthesis of MoS_2 /CNH was performed by dissolving ammonium molybdate (1 mM, 10 ml) and thioacetamide (2, 5, 10, 30 and 40 mM, 10 ml) in an aqueous dispersion of acid-treated CNH (0.5 mg/ml, 10 ml) under vigorous stirring. Then, the dispersion was transferred into a Teflon-lined stainless-steel autoclave and maintained at 180 °C. After 15 h, the reaction system was allowed to cool down to room temperature. The product (MoS_2 /CNH) was washed with water and absolute ethanol for several times and dried at 60 °C under vacuum. The MoS_2 without CNH was synthesized using similar procedure.

PdCl_2 (1 mg) was dissolved in 1 M HCl solution (200 μl) and added to aqueous solutions containing DA (0.2, 0.5 and 1.0 mg/ml, 5 ml). The yellow solution was allowed to stir 5 min and pH was adjusted from 2 to around pH 8 to 9. The yellow solution became dark brown, indicating the polymerization reaction of DA. The solution was stirred for 12 h and NaBH_4 (4 mg) was added. Then the deep brown solution became black. This reduction reaction was

allowed for 15 min to obtain the polydopamine-stabilized Pd NPs (PDA-Pd(0)). The product was centrifuged and washed with water several times. For the synthesis of PDA-Pd/CNH composite, the acid-treated CNH was mixed with PdCl_2 and sonicated for 30 min. Then the dopamine solution (0.2 mg/ml, 5 ml) was introduced to this dispersion of CNH and PdCl_2 . The further step was same as the synthesis procedure of PDA-Pd(0). Finally, the obtained PDA-Pd(0) and PDA-Pd/CNH composites were re-dispersed in water by sonicating for 1 h. These dispersions were used as electrocatalysts.

2.3. Electrochemical experiments

The electrochemical HER measurements were carried out on a electrochemical workstation (model HZ-3000 automatic polarization system, Hokuto Denco, Japan) using a conventional three electrode work station: A well-polished glassy carbon working electrode (GCE) (Anatech Co., Ltd, Taiwan), an Ag|AgCl reference electrode and a platinum wire counter electrode were employed. Accordingly, the electrochemical HER in this cell was monitored by the linear sweep voltammetry (LSV) and the HER-occurring potential was converted to the reversible hydrogen electrode (RHE) potential. A dispersion (5 μl) of synthesized electrocatalysts, which were beforehand well dispersed in water by means of ultra-sonication (Bransonic Ultrasonics Model B1210J-DTH, Japan) for 15 min, was drop-casted on a GCE surface and dried at room temperature. Subsequently, an ethanol solution of Nafion (0.5 vol%, 2 μl) was dried on the electrode surface to immobilize electrocatalysts on the electrode. While the measuring of HER, the electrolyte solutions were maintained at the stirring condition, since the MoS_2 /CNH electrodes generated hydrogen bubbles.

3. Results and discussion

3.1. Contribution of CNH on MoS_2

In-situ hydrothermal method was applied to synthesize MoS_2 on CNH surface. Fig. 1A(a) shows the TEM image of as-synthesized MoS_2 , which confirmed the ultrathin sheet or the flake-like structure. The morphology of synthesized MoS_2 /CNH in Fig. 1A(b) displayed also sheet or flake which was derived from MoS_2 and coexisted with globular CNH. The fact that the MoS_2 does not encapsulate the CNH indicates the weak interaction between MoS_2 and CNH.

The electrochemical HER behavior of MoS_2 was investigated using LSV in an acidic condition. Here the molar ratio of ammonium molybdate and thioacetamide was kept at 1:10. For monitoring the HER efficiency, rich sulfur atoms produce more active sites in MoS_2 sheet and may result in the enhanced HER activity [42]. The pristine MoS_2 produced hydrogen at the onset potential of 185 mV and reached the current density of 10 mA/cm² at the overpotential of 286 mV (Fig. 1B). In this connection, the MoS_2 /CNH generated hydrogen at the onset potential of 165 mV and attained the current density of 10 mA/cm² at 246 mV (Fig. 1B). Hence, it should be mentioned that the coexistence of CNH minimized about 20 mV of the HER onset potential and enhanced the current density. Moreover, the Tafel slope values for MoS_2 (92 mV dec⁻¹) and MoS_2 /CNH (86 mV dec⁻¹) (Fig. 1C) depend on the HER kinetics and mechanism. This result reveals that the HER activity of MoS_2 is enhanced slightly due to the CNH. However, compared to the previous reports used MoS_2 -carbon composite [36,37], the HER efficiency in the present work is too low. Therefore, the composite of CNH with another metal nanoparticle was selected to improve the efficiency of metal nanoparticle.

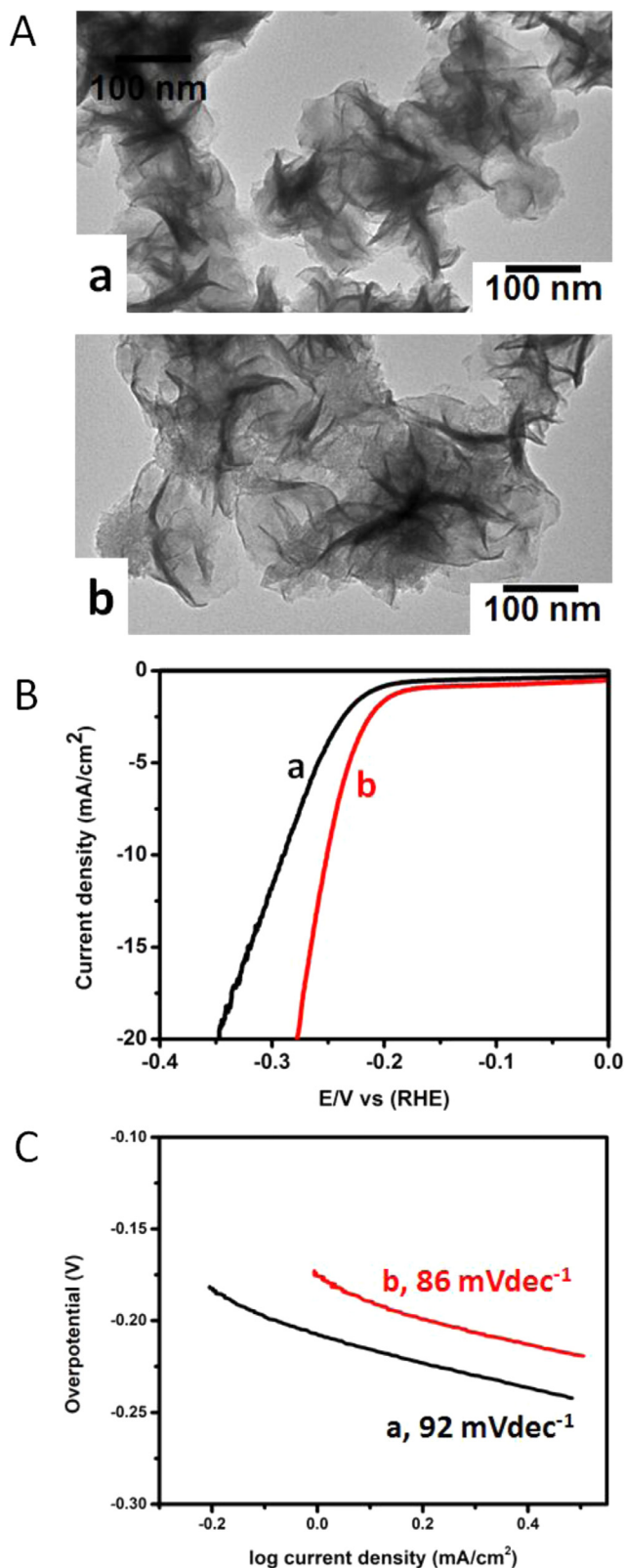


Fig. 1. A) TEM images, B) electrochemical HER polarization curve in 0.5M H₂SO₄ electrolyte solution and C) Tafel plots for a) MoS₂ and b) MoS₂/CNH.

Table 1

FT-IR absorption bands (in cm⁻¹) and their assignments of CNH, PDA and PDA-Pd/CNH.

Assignment	Acid-treated CNH	PDA*	PDA-Pd/CNH
ν OH	3490	–	3475
ν N–H	–	3379	–
ν C=O	1726	–	1710
ν C=C	1586	1627	1580
ν C=N	–	1512	1506
ν C–O	1225	–	1205

* Data from Luo et al. [45].

3.2. Contribution of CNH on PDA encapsulated Pd NPs

When DA was mixed with PdCl₂ dissolved in acidic solution, the Pd ions form DA-PdCl₂ complex with DA. The oxidation and self-polymerization process of DA-PdCl₂ complex were occurred at basic condition (>8). It is worth noting that while DA was oxidized into dopamine-quinone under the basic condition, the two-electrons transfer reaction happened, the released electrons could reduce the Pd ions to Pd metals and, at the same time, DA became PDA within 4–5 h [43]. Finally, the reduced metal particles were completely encapsulated in PDA domains.

On the other hand, the synthesis of PDA-Pd/CNH composite was initiated by mixing of CNH with PdCl₂ and, then DA was added for polymerization on PdCl₂-CNH. Here, PDA encapsulated the CNH-Pd ion complex and reduced Pd ions to Pd(0). However, the addition of NaBH₄ completed the reduction of any non-reduced Pd ions. The TEM images of PDA-Pd, PDA-Pd(0) and PDA-Pd/CNH are displayed in Fig. 2. Pd NPs reduced by PDA were completely encapsulated within PDA, and their particle size was less than 5 nm (Fig. 2A). The morphology of PDA-Pd(0) was different from PDA-Pd, which was taken before the addition of NaBH₄. The cubic-like PDA-Pd(0) was formed by reducing PDA-Pd ion with NaBH₄. Each cubic Pd(0)NPs were separately encapsulated by PDA (Fig. 2B). As seen in Fig. 2C, the Pd NPs were well anchored on CNH, distributed without aggregation and coated by PDA. The average size of Pd NPs was found around 3.5 ± 0.5 nm using TEM particle size analyzer. This result reveals that the PDA on CNH plays a role as a protector of Pd NPs from aggregation as well as a size controller. The PDA completely covered the Pd/CNH with keeping the spherical shape of CNH, when the content of DA was high (1 mg/ml) (Fig. 2D).

The complexation of PDA and Pd NPs was confirmed by the UV-visible absorption spectroscopic study. In Fig. 3A and B, the absorption bands of DA at 204, 225 and 280 nm reflected π - π^* transition of aromatic ring [44], while Pd(II) ion displayed the bands at 222 and 280 nm, characteristic to Pd ion in acidic solution [45]. Then, the broad band at 434 nm was assigned to d-d transition of Pd ion in the acidic solution [42,46]. Then, the absorption bands of DA-PdCl₂ mixture at 215, 280 and 434 nm (around pH 1.5, 5 min reaction time) indicated the coexistence of DA and Pd ions in the solution. It is worth noting that, upon addition of NaBH₄, the disappearance of absorption bands of both DA and Pd(II) ion and the appearance of a weak absorption band at 280 nm indicated the polymerization of DA and the reduction of Pd ion on CNH.

An existence of PDA in PDA-Pd/CNH was further confirmed by FT-IR spectroscopy in Fig. 3C, and wavenumber and assignment of IR bands were listed in Table 1. The characteristic bands of CNH appeared at 3490, 1726, 1586 and 1225 cm⁻¹ corresponding to OH, C=O, C=C and C–O stretching vibration modes, respectively. Based on the earlier report [47], the PDA exhibited three bands at 3379, 1627 and 1512 cm⁻¹ assigned to N–H, C=C and C=N stretching modes, respectively. Meanwhile, the FT-IR bands of PDA-Pd/CNH possessed one additional shoulder band at 1506 cm⁻¹ from PDA

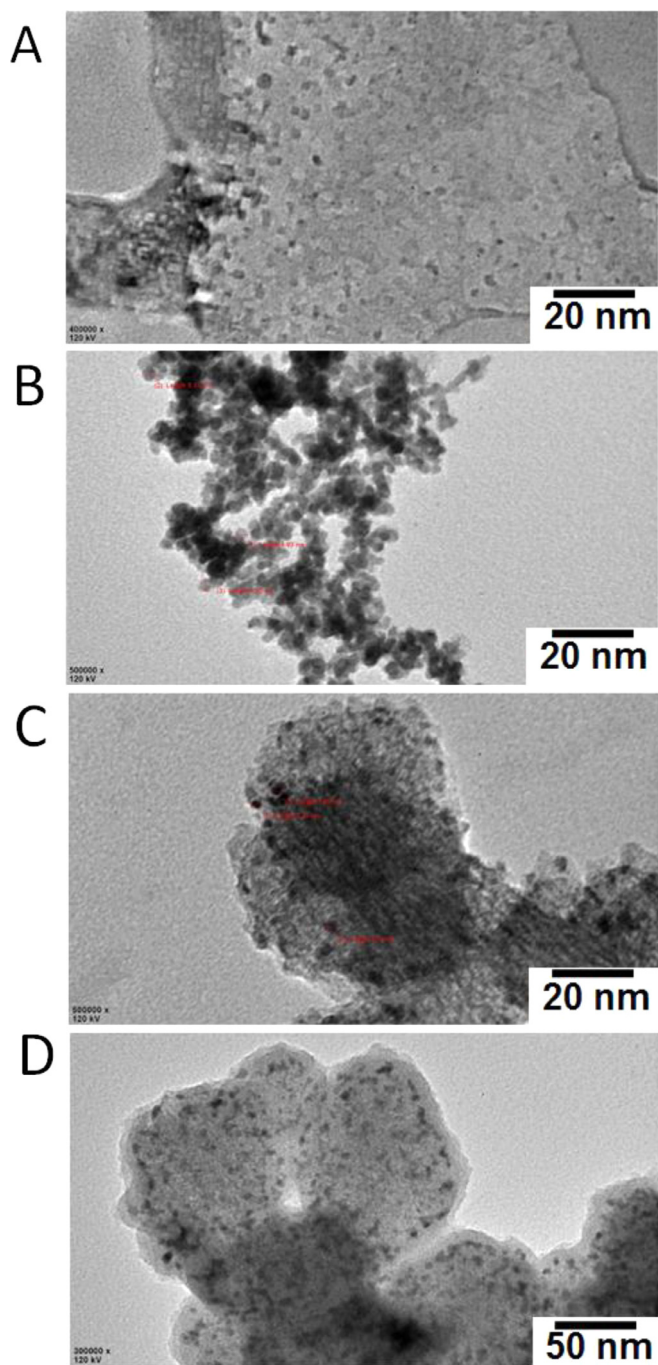


Fig. 2. TEM images of A) PDA (0.2 mg/ml) encapsulated Pd NPs, B) PDA-Pd(0) (0.2 mg/ml), C) PDA (0.2 mg/ml) coated Pd/CNH and D) PDA (1 mg/ml) coated Pd/CNH.

besides characteristic absorption bands of CNH, indicating the co-existence of PDA and CNH.

Further, the existence of Pd NPs was confirmed based on XRD patterns and XPS analyses. The XRD patterns of CNH, PDA-Pd(0) and PDA-Pd/CNH are displayed in Fig. 4A. The XRD pattern of CNH showed a peak at 2θ value of 26° , which corresponds to the graphitic (002) plane of SWCNH. The broad peak between 25 and 30° for PDA-Pd(0) indicates the amorphous structure or the small size of PDA. Besides, another peak at 40° corresponds to a (111) plane of Pd NPs fcc crystal. Owing to the PDA encapsulation, weak peaks of Pd(0) were appeared in the PDA-Pd(0). However, the PDA-Pd/CNH composite exhibited one intense peak at 33° , which could

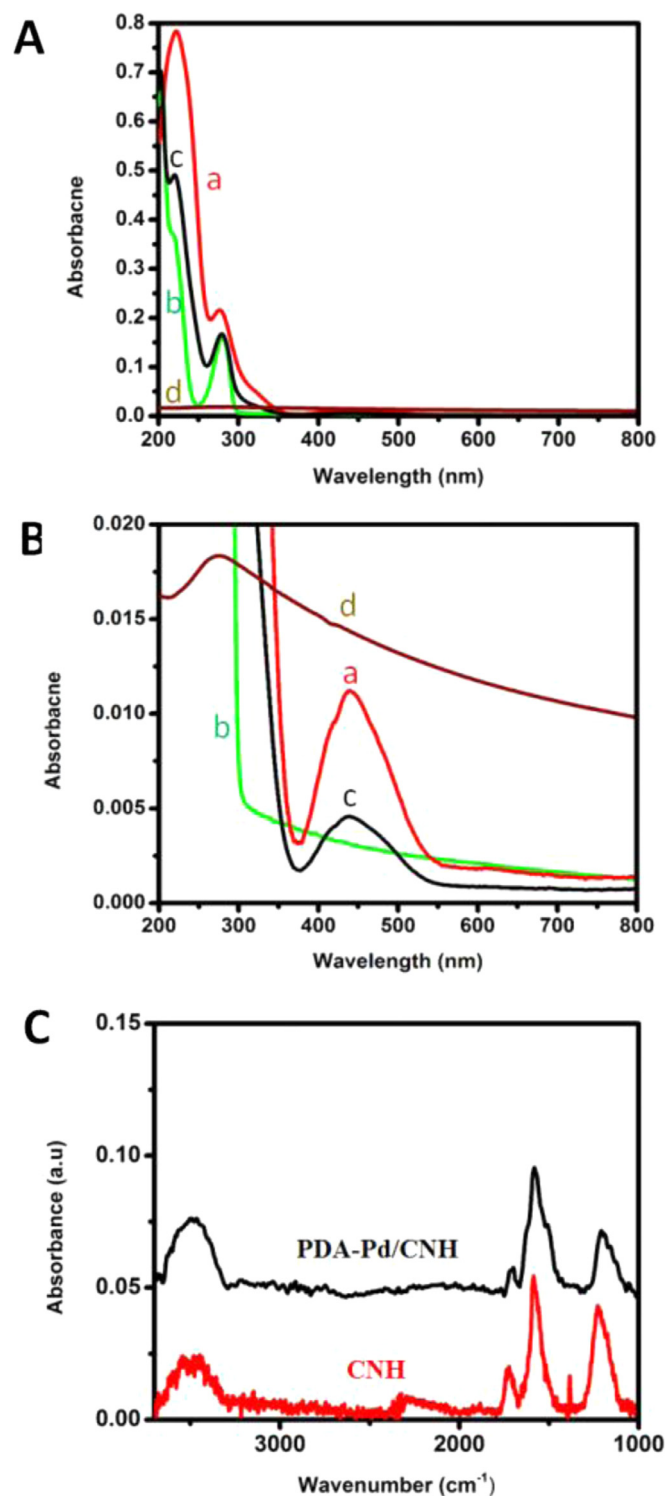


Fig. 3. A) & B) UV-vis absorption spectra of a) PdCl₂, b) DA, c) DA-PdCl₂ and d) PDA-Pd/CNH. C) FT-IR absorption spectra of PDA-Pd/CNH and CNH.

be due to the substrate used for XRD measurement. A broad peak at 25 – 30° is indicating the existence of amorphous or small PDA in the PDA-Pd/CNH. Besides, the peaks at 34 and 57° represent (002) and (112) planes of PdO, respectively [48,49], and a peak at 48° corresponds to a (200) plane of Pd NPs. These results indicate the coexistence of Pd(0) and PdO in the PDA-Pd/CNH.

The existence of elements in the composite of PDA-Pd/CNH was confirmed from XPS analysis (Fig. 4B) and the deconvoluted

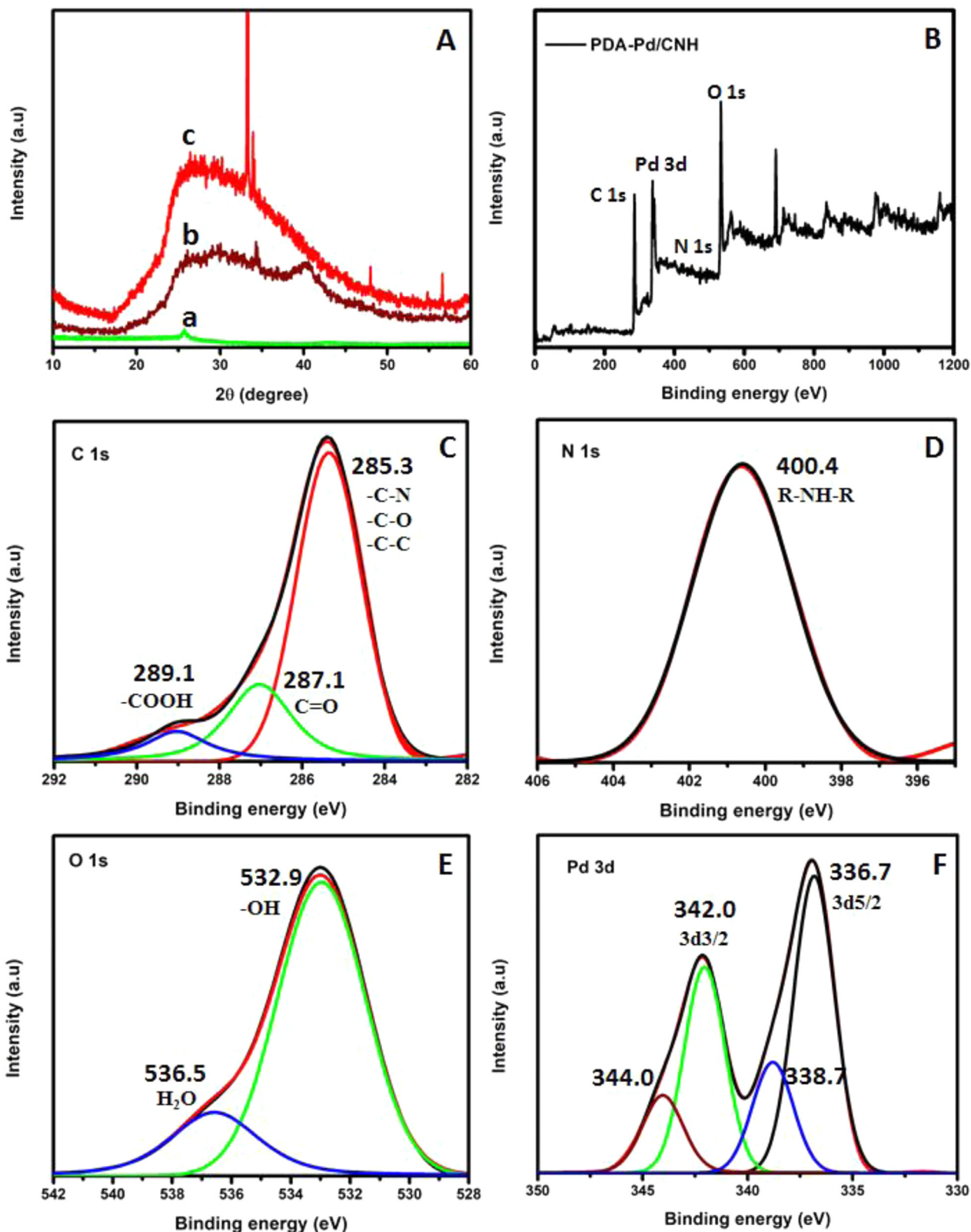


Fig. 4. A) XRD patterns of a) CNH, b) PDA-Pd(0) and c) PDA-Pd/CNH, B) XPS chart of PDA-Pd/CNH, C) C 1s, D) N 1s, E) O 1s and F) Pd 3d peaks of XPS chart.

spectra (Fig. 4C–F). The XPS displayed C1s, N1s, O1s and Pd3d peaks of PDA-Pd/CNH. Fig. C–F indicates high resolution spectra of individual elements in the PDA-Pd/CNH. The peaks were assigned to corresponding functional groups as inserted in Fig. C–F. The deconvoluted C1s peak represents the presence of C–N, C–O and C–C

groups in the PDA-Pd/CNH. The N1s peak at 400.4 eV is assigned to R-NH-R group of PDA. The peak at 532.9 eV indicates that OH group is present in the as-synthesized composite. The additional peak of O1s at 536.5 eV is likely due to the adsorption of water molecule in the composite. A pair of peaks at 336.7 and 342.0 eV

correspond to Pd 3d_{5/2} and Pd 3d_{3/2} [50, 51]. The intense and weak peaks indicate the co-existence of Pd(0) and Pd²⁺, respectively, in the PDA-Pd/CNH. The co-existence of Pd²⁺ with Pd(0) is consistent with the observation of PdO Bragg peaks in XRD of PDA-Pd/CNH.

3.3. Electrochemical HER efficiency of PDA-Pd/CNH

The electrochemical HER efficiency was examined using a three-electrode system and by recording cyclic voltammogram in a 0.5 M H₂SO₄ electrolyte solution. Fig. 5A shows the HER polarization curve. It indicated that both PDA-Pd/CNH and PDA-Pd(0)-modified electrodes produced hydrogen at overpotential of -10 mV/s, but the PDA-Pd ion-modified electrode displayed poor HER activity in comparison with PDA-Pd(0), while the commercial 40 wt% Pt/C HER electrode occurred at the overpotential 0 mV [6]. These results reveal that the reduction of Pd ion to Pd(0) was partially proceeded by PDA (as indicated by UV-vis absorption study), since PDA has potential to reduce noble metals [43]. However, the further addition of a strong reducer such as NaBH₄ promoted the activity of PDA-Pd. Furthermore, the addition of CNHs enhanced the cathodic current density towards hydrogen evolution: The PDA-Pd/CNH exhibited the current density of -10 mA/cm² at 100 mV/s.

The control of the amount of DA is significant on improvement of HER efficiency. Fig. 5B depicts the HER polarization curve at different amounts of PDA against Pd NPs. As described in TEM characterization, 1.0 mg/ml of DA produced the thicker covering on Pd/CNH than 0.2 mg/ml of DA. However, the large amount of DA caused the low electron transfer rate towards HER (Fig. 5B). This result reveals that the thick coating by PDA diminishes the electron transfer rate of Pd NPs during HER. To confirm the reaction mechanism of electrocatalysis, the Tafel slope obtained from LSV polarization curve is mostly employed. Fig. 5C displays the Tafel slope plots of PDA-Pd(0) and PDA-Pd/CNH. The theoretical Tafel slope value is assessed as ~120, ~40 and ~30 mV/decade corresponding to Volmer reaction, Heyrovsky reaction and Tafel reaction, respectively. These three possible reactions have generally been suggested for HER in acidic media [52].

$\text{H}_3\text{O}^+ + \text{e}^- \rightarrow \text{H}_{\text{adsorbed}} + \text{H}_2\text{O}$. ----- (Volmer reaction, discharge step)

$\text{H}_{\text{adsorbed}} + \text{H}_3\text{O}^+ + \text{e}^- \rightarrow \text{H}_2 + \text{H}_2\text{O}$, ----- (Heyrovsky, desorption step) or

$\text{H}_{\text{adsorbed}} + \text{H}_{\text{adsorbed}} \rightarrow \text{H}_2$. ----- (Tafel reaction, recombination step)

Compared to the slope value of PDA-Pd(0) (111 mV/decade), the PDA-Pd/CNH exhibited small Tafel slope value (61 mV/decade), although the commercial Pt/C exhibited the Tafel value of 36 mV/decade. Based on theoretical value, the HER on the PDA-Pd/CNH electrode proceeded through the Volmer–Heyrovsky mechanism. It is well known that the commercial Pt/C reaction follows the Volmer–Tafel mechanism. Hence, the reaction mechanism on PDA-Pd/CNH was different from the commercial Pt/C. The HER efficiency of PDA-Pd/CNH is compared with other Pd NPs related reports as listed in Table 2. It can be seen that the HER onset potential is lower than other carbon based Pd NPs. Besides, the current density is higher than Pd-CoCNT modified electrode. Relating to the reported materials such as Pd₅₀Ru₅₀/CNs and Pt_{0.5}Pd_{0.5}NPs/PEDOT-SG/GCE, the current density of PDA-Pd/CNH is considerably lower. Moreover, these composites need bi-metals and high costs for preparation. However, the Tafel slope values of Pd-CoCNT and Pt_{0.5}Pd_{0.5}NPs/PEDOT-SG/GCE are 56 and 57 mV/dec, respectively, specifying Volmer–Heyrovsky mechanism. Hence, the

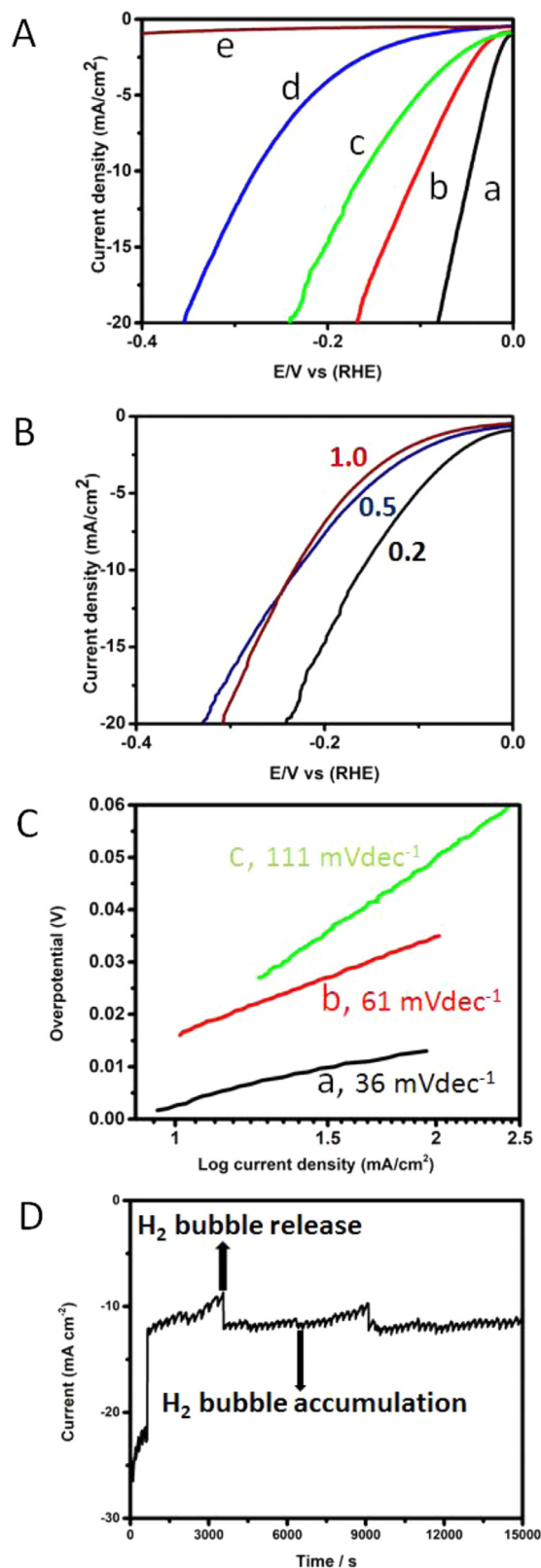


Fig. 5. Electrochemical HER polarization curves in a 0.5 M H₂SO₄ electrolyte solution A) at various electrodes of a) Pt/C, b) PDA-Pd/CNH, c) PDA-Pd(0), d) PDA-Pd ion and e) CNH, B) at different amounts (0.2, 0.5 and 1.0 mg) of PDA-Pd(0), C) Tafel plots for a) Pt/C, b) PDA-Pd/CNH and c) PDA-Pd(0) and D) HER current-time curve of PDA-Pd/CNH in 0.5 M H₂SO₄.

Table 2
Comparison of HER results of present electrocatalysts to other noble metal electrocatalysts.

Electrocatalyst	Onset potential (mV)	Over potential at 10 mA/cm ² Current density	Tafel slope (mV dec ⁻¹)	Reference
MoS ₂ /CNH	165	246	86	This work
MoS ₂	185	286	92	
PDA-Pd/CNH	10	100	61	This work
PDA-Pd(0)	10	185	111	
Pd-rGO	-380	-	122 mV	[53]
Pd ₅₀ Ru ₅₀ / ^a CNs	-37.3	45.1	-	[54]
Pd-CoCNT	-24 mV	112	56	[55]
Pt _{0.5} Pd _{0.5} NPs/PEDOT- ^b SG/GCE	0.172 vs _{Ag/AgCl}	-	57	[56]
Ag/Pd/ ^c CILE	-0.27 vs _{Ag/AgCl}	-	156	[57]

a- Carbon Nanosheets, b- sulfonated graphene and c- carbon ionic liquid electrode.

HER mechanism of present report is similar with other noble metal catalysts.

Moreover, the oxidized CNH has the inherent defect structure, the internal nanospace and the extrinsic pores, which provide preferable active sites for the Pd nanoparticle [58,59]. The peculiar properties and the inherent defect structure of CNH enable the uniform dispersion and the firm anchoring of Pd NPs as confirmed by TEM images (Fig. 2C and D), which facilitated the synergistic effect as well as the HER activity [59]. The defective carbon in CNH can promote the diffusion as well as adsorption of protons on the Pd/CNH surface, facilitating the Volmer–Heyrovsky mechanism (Tafel slope = 61 mV/dec) for the production of hydrogen. In contrast, MoS₂ sheets completely wrapped the CNH surface and limited the exposure of defective carbon to the electrolyte (see Fig. 1Ab). Further, CNHs made of single layer of graphene in the shape of horns are likely to be agglomerated through van der Waals attraction upon wrapping with MoS₂ sheets [60]. As a result, the active defective sites in CNH are likely to be blocked by MoS₂, which led to poor protons transport, less efficient protons diffusion, minimum or less synergistic effect and thus poor production of hydrogen. This is evident in a relatively larger Tafel slope of 86 mV/dec. The production of hydrogen at the MoS₂/CNH surface has thus proceeded through the well-known Tafel reaction pathway and not through Volmer–Heyrovsky mechanism as that of Pd/CNH.

The HER polarization curves of PDA-Pd/CNH at the first scan and the scan after 500 cycles was monitored using LSV. The onset potential and the current density for HER activity stood same after 500 cycles (data not shown). This result indicates that the PDA-Pd/CNH-modified electrode maintains the excellent stability. Moreover, non-cleavable ability of the composites during HER reveals the superior durability nature. Finally, the chronoamperometry was employed at constant potential (-0.1 V vs RHE) to measure the stability of PDA-Pd/CNH modified electrode. It can be seen in Fig. 5D for HER current density versus time that the continuous HER process occurred, and the corresponding plot displayed its stability: The current density conserved identical for 4 h. This fact reveals the excellent durability of PDA-Pd/CNH modified electrode.

To clarify the effects of MoS₂ to HER activity of Pd nanoparticles, the HER activities of MoS₂, MoS₂/CNH, commercial catalyst (Pd on activated carbon) and synthesized Pd on CNH are provided as controls in Fig. 6. Related to MoS₂, the MoS₂/CNH exhibits better HER activity in terms of onset potential (-165 mV vs. RHE) and overpotential (-246 mV vs. RHE) to reach 10 mAcm⁻². Compared to benchmark commercial catalyst (Pd on activated carbon), synthesized Pd on CNH exhibits excellent HER activity. Its onset potential is relatively low (-6 mV vs. RHE) and the overpotential (-124 mV vs. RHE) to reach 10 mAcm⁻² is minimum. The results of control experiments clearly revealed that CNH acts as a viable carbon support for both MoS₂ and Pd, enhancing charge and mass transports as well as their HER performances through improved interfacial contacts with its defective carbons. We have encapsu-

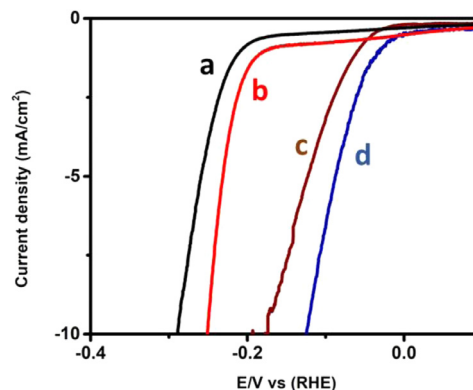


Fig. 6. Electrochemical HER polarization curves of control electrodes in a 0.5M H₂SO₄ electrolyte solution. a) MoS₂, b) MoS₂/CNH, c) commercial catalyst (Pd on activated carbon) and d) synthesized Pd on CNH.

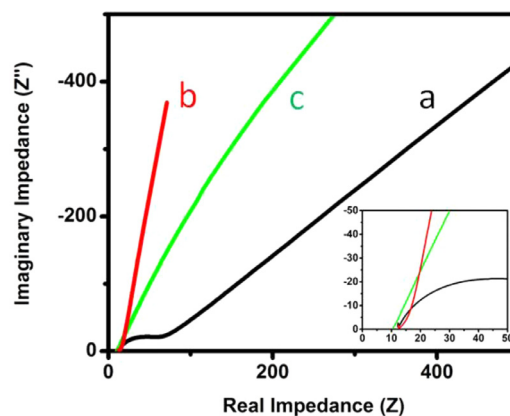


Fig. 7. Impedance spectra of (a) bare electrode, (b) PDA-Pd/CNH and (c) PDA-Pd.

lated PDA with Pd/CNH to avoid the reversible oxidation nature of sole Pd metal nanoparticle mainly for improving the stability. It is worth noting that the HER activity of Pd/CNH is still retained even after encapsulation of PDA.

To assess the CNH electron transfer rate, the electrochemical impedance spectrum (EIS) measurement was performed. The Randles circuit model was applied to calculate the electron transfer resistance (R_{ct}) of modified electrodes. In Fig. 7, the unmodified (bare) electrode displayed a semicircle, indicating the poor electron transfer rate. However, the PDA-Pd/CNH-modified electrode exhibited small R_{ct} value (3.6 Ω) than PDA-Pd-modified electrode (7.8 Ω), revealing that excellent electron transfer of PDA-Pd/CNH-modified electrode. Thus, the CNH enhances the electron transfer rate of PDA-Pd NPs for HER reaction due to its excellent electric conductivity nature of CNH [6]. The EIS curves of PDA-Pd/CNH electrodes fabricated with two different PDA coatings (0.2 mg/ml and 1 mg/ml) were also compared. Note that the slope of thin

PDA layer coated electrode in the low frequency region is larger than that of the electrode with thick PDA coating, suggesting that thin PDA coating results in lower diffusive resistance and faster ion transport. These EIS results further support our reasoning that increasing PDA coating thickness decreases the proton transport and the diffusion kinetics and results in poor HER activity.

4. Conclusions

The CNH enhanced the HER efficiency of MoS₂- and PDA/Pd NPs-modified electrodes. Nevertheless, the HER efficiency of MoS₂/CNH-modified electrode is still low, since the poor interaction of MoS₂ and CNH. However, the contribution of CNH to PDA-Pd indicates the more superior HER activity than MoS₂/CNH. The nanosized Pd NPs (> 5 nm) are highly distributed to the CNH surface without aggregation, and the thin coating of PDA reduces the inhibition for the reversible oxidation nature of Pd NPs. Thus, the thinner coating of H₂ adsorbent (Pd) by protector (PDA on PDA-Pd/CNH) exhibits higher HER current density than thicker coating. The reported result evidently shows that CNH-based composites are the excellent choice to enhance the HER activity of metal particles and other nanomaterials.

Acknowledgments

This work was partially supported by a grant of Ministry of Science and Technology (MOST 104-2221-E-011-003), Taiwan. BD appreciates the financial support from National Taiwan University of Science and Technology, Taiwan, for postdoctoral scholarship.

References

- [1] Hosseini SE, Wahid MA. Hydrogen production from renewable and sustainable energy resources: promising green energy carrier for clean development. *Renew Sustain Energy Rev* 2016;57:850–66.
- [2] Bicelli LP. Hydrogen: a clean energy source. *Int J Hydrog Energy* 1986;11(9):555–62.
- [3] Morales-Guio CG, Stern L-A, Hu X. Nanostructured hydrotreating catalysts for electrochemical hydrogen evolution. *Chem Soc Rev* 2014;43(18):6555–69.
- [4] Liu K, Zhong H, Meng F, Zhang X, Yan J, Jiang Q. Recent advances in metal–nitrogen–carbon catalysts for electrochemical water splitting. *Mater Chem Front* 2017;1(11):2155–73.
- [5] Roger I, Shipman MA, Symes MD. Earth-abundant catalysts for electrochemical and photoelectrochemical water splitting. *Nat Rev Chem* 2017;1(1):0003.
- [6] Devadas B, Imae T. Hydrogen evolution reaction efficiency by low loading of platinum nanoparticles protected by dendrimers on carbon materials. *Electrochem Commun* 2016;72:135–9.
- [7] Chen WF, Sasaki K, Ma C, Frenkel AI, Marinkovic N, Muckerman JT, Zhu Y, Adzic RR. Hydrogen-evolution catalysts based on non-noble metal nickel–molybdenum nitride nanosheets. *Angew Chem Int Ed* 2012;51(25):6131–5.
- [8] Hua S, Qu D, An L, Xi G, Chen G, Li F, Zhou Z, Sun Z. Highly dispersed few-layer MoS₂ nanosheets on S, N co-doped carbon for electrocatalytic H₂ production. *Chinese J Catal* 2017;38(6):1028–37.
- [9] Sun Y, Shi G. Graphene/polymer composites for energy applications. *J Polym Sci B* 2013;51(4):231–53.
- [10] Gopi CVM, Ravi S, Rao SS, Reddy AE, Kim H-J. Carbon nanotube/metal-sulfide composite flexible electrodes for high-performance quantum dot-sensitized solar cells and supercapacitors. *Sci Rep* 2017;7:46519.
- [11] Mondal A, Jana NR. Graphene-nanoparticle composites and their applications in energy, environmental and biomedical science. *Rev Nanosci Nanotechnol* 2014;3(3):177–92.
- [12] Siriviriyannun A, Imae T, Calderó G, Solans C. Phototherapeutic functionality of biocompatible graphene oxide/dendrimer hybrids. *Colloids Surf B Biointerfaces* 2014;121:469–73.
- [13] Bianco A, Kostarelos K, Partidos CD, Prato M. Biomedical applications of functionalised carbon nanotubes. *Chem Comm* 2005;5:571–7.
- [14] Siriviriyannun A, Popova M, Imae T, Kiew LV, Looi CY, Wong WF, Lee HB, Chung LY. Preparation of graphene oxide/dendrimer hybrid carriers for delivery of doxorubicin. *Chem Eng J* 2015;281:771–81.
- [15] Candelaria SL, Shao Y, Zhou W, Li X, Xiao J, Zhang J-G, Wang Y, Liu J, Li J, Cao G. Nanostructured carbon for energy storage and conversion. *Nano Energy* 2012;1(2):195–220.
- [16] Devadas B, Imae T. Effect of carbon dots on conducting polymers for energy storage applications. *ACS Sustain Chem Eng* 2018;6:127–34.
- [17] Ahmed MM, Imae T. Electrochemical properties of a thermally expanded magnetic graphene composite with a conductive polymer. *Phys Chem Chem Phys* 2016;18(15):10400–10.
- [18] Mani V, Devadas B, Chen S-M. Direct electrochemistry of glucose oxidase at electrochemically reduced graphene oxide-multiwalled carbon nanotubes hybrid material modified electrode for glucose biosensor. *Biosens Bioelectron* 2013;41:309–15.
- [19] Siriviriyannun A, Imae T, Nagatani N. Electrochemical biosensors for biocontaminant detection consisting of carbon nanotubes, platinum nanoparticles, dendrimers, and enzymes. *Anal Biochem* 2013;443(2):169–71.
- [20] Zhang L, Xiao J, Wang H, Shao M. Carbon-based electrocatalysts for hydrogen and oxygen evolution reactions. *ACS Catal* 2017;7(11):7855–65.
- [21] Siriviriyannun A, Imae T. Advantages of electrodes with dendrimer-protected platinum nanoparticles and carbon nanotubes for electrochemical methanol oxidation. *Phys Chem Chem Phys* 2013;15(14):4921–9.
- [22] Zhou W, Jia J, Lu J, Yang L, Hou D, Li G, Chen S. Recent developments of carbon-based electrocatalysts for hydrogen evolution reaction. *Nano Energy* 2016;28:29–43.
- [23] Li Y, Wang H, Xie L, Liang Y, Hong G, Dai H. MoS₂ nanoparticles grown on graphene: an advanced catalyst for the hydrogen evolution reaction. *J Am Chem Soc* 2011;133(19):7296–9.
- [24] Yan Y, Ge X, Liu Z, Wang J-Y, Lee J-M, Wang X. Facile synthesis of low crystalline MoS₂ nanosheet-coated CNTs for enhanced hydrogen evolution reaction. *Nanoscale* 2013;5(17):7768–71.
- [25] Zhu S, Xu G. Single-walled carbon nanohorns and their applications. *Nanoscale* 2010;2(12):2538–49.
- [26] Zhu C, Liu D, Chen Z, Li L, You T. Superior catalytic activity of Pt/carbon nanohorns nanocomposites toward methanol and formic acid oxidation reactions. *J Colloid Interface Sci* 2018;511:77–83.
- [27] Karousis N, Suarez-Martinez I, Ewels CP, Tagmatarchis N. Structure, properties, functionalization, and applications of carbon nanohorns. *Chem Rev* 2016;116(8):4850–83.
- [28] Zhu G, Sun H, Zou B, Liu Z, Sun N, Yi Y, Wong K-y. Electrochemical sensing of 4-nitrochlorobenzene based on carbon nanohorns/graphene oxide nanohybrids. *Biosens Bioelectron* 2018;106:136–41.
- [29] Gao Z, Liu X, Zhang C, Tang Z, Chen J, Yu C. Electrochemical immunosensor for monocyte chemoattractant protein-1 detection based on Pt nanoparticles functionalized single-walled carbon nanohorns. *Int J Electrochem Sci* 2018;13:3923–34.
- [30] Mounfield WP, Garg A, Shao-Horn Y, Román-Leshkov Y. Electrochemical oxygen reduction for the production of hydrogen peroxide. *Chem* 2018;4(1):18–19.
- [31] Chang CC, Imae T. Synergistic performance of composite supercapacitors between carbon nanohorn and conducting polymer. *ACS Sustain Chem Eng* 2018;6(4):5162–72.
- [32] Cheng Y, Lu S, Liao F, Liu L, Li Y, Shao M. Rh-MoS₂ nanocomposite catalysts with Pt-like activity for hydrogen evolution reaction. *Adv Funct Mater* 2017;27(23):1700359.
- [33] Laursen AB, Kegnes S, Dahl S, Chorkendorff I. Molybdenum sulfides—efficient and viable materials for electro- and photoelectrocatalytic hydrogen evolution. *Energy Environ Sci* 2012;5(2):5577–91.
- [34] Merki D, Vruble H, Rovelli L, Fierro S, Hu X, Fe Co. and Ni ions promote the catalytic activity of amorphous molybdenum sulfide films for hydrogen evolution. *Chem Sci* 2012;3(8):2515–25.
- [35] Merki D, Hu X. Recent developments of molybdenum and tungsten sulfides as hydrogen evolution catalysts. *Energy Environ Sci* 2011;4(10):3878–88.
- [36] Wang T, Liu L, Zhu Z, Papakonstantinou P, Hu J, Liu H, Li M. Enhanced electrocatalytic activity for hydrogen evolution reaction from self-assembled monodispersed molybdenum sulfide nanoparticles on an Au electrode. *Energy Environ Sci* 2013;6(2):625–33.
- [37] Huang H, Huang W, Yang Z, Huang J, Lin J, Liu W, Liu Y. Strongly coupled Mo₂ nanoflake–carbon nanotube nanocomposite as an excellent electrocatalyst for hydrogen evolution reaction. *J Mater Chem A* 2017;5(4):1558–66.
- [38] Yang L, Zhou W, Lu J, Hou D, Ke Y, Li G, Tang Z, Khang X, Chen S. Hierarchical spheres constructed by defect-rich MoS₂/carbon nanosheets for efficient electrocatalytic hydrogen evolution. *Nano energy* 2016;22:490–8.
- [39] Zhou W, Zhou K, D Hou, Liu X, Li G, Sang Y, Liu H, Li L, Chen S. Three-dimensional hierarchical frameworks based on MoS₂ nanosheets self-assembled on graphene oxide for efficient electrocatalytic hydrogen evolution. *ACS Appl Mater Interfaces* 2014;6:21534–40.
- [40] Mahesh KN, Balaji R, Dhathathreyan K. Palladium nanoparticles as hydrogen evolution reaction (HER) electrocatalyst in electrochemical methanol reformer. *Int J Hydrogen Energy* 2016;41(1):46–51.
- [41] Ghaseini S, Hosseini SR, Nabipour S, Asen P. Palladium nanoparticles supported on graphene as an efficient electrocatalyst for hydrogen evolution reaction. *Int J Hydrogen Energy* 2015;40(46):16184–91.
- [42] Zhu H, Du M, Zhang M, Zou M, Yang T, Wang S, Yao J, Guo B. S-rich single-layered MoS₂ nanoplates embedded in N-doped carbon nanofibers: efficient co-electrocatalysts for the hydrogen evolution reaction. *Chem Commun* 2014;50(97):15435–8.
- [43] Liu Y, Ai K, Lu L. Polydopamine and its derivative materials: synthesis and promising applications in energy, environmental, and biomedical fields. *Chem Rev* 2014;114(9):5057–115.
- [44] Mostovaya O, Padnya P, Vavilova A, Shurpik D, Khairutdinov B, Mukhametzyanov T, Khannanov A, Kutyreva M, Stoikov I. Tetracarboxylic acids on a thiacalixarene scaffold: synthesis and binding of dopamine hydrochloride. *New J Chem* 2018;42(1):177–83.
- [45] Elding LI. Palladium (II) halide complexes. I. Stabilities and spectra of palladium (II) chloro and bromo aqua complexes. *Inorg Chim Acta* 1972;6:647–51.

- [46] Espinosa-Alonso L, De Jong K, Weckhuysen B. A UV-vis micro-spectroscopic study to rationalize the influence of Cl⁻(aq) on the formation of different Pd macro-distributions on γ -Al₂O₃ catalyst bodies. *Phys Chem Chem Phys* 2010;12(1):97–107.
- [47] Luo H, Gu C, Zheng W, Dai F, Wang X, Zheng Z. Facile synthesis of novel size-controlled antibacterial hybrid spheres using silver nanoparticles loaded with poly-dopamine spheres. *RSC Adv* 2015;5(18):13470–7.
- [48] Wojcieszak R, Genet MJ, Eloy P, Ruiz P, Gaigneaux EM. Determination of the size of supported Pd nanoparticles by x-ray photoelectron spectroscopy. Comparison with x-ray diffraction, transmission electron microscopy, and H₂ chemisorption methods. *J Phys Chem C* 2010;114:16677–84.
- [49] Sekiguchi Y, Hayashi Y, Takizawa H. Synthesis of palladium nanoparticles and palladium/spherical carbon composite particles in the solid-liquid system of palladium oxide-alcohol by microwave irradiation. *Mater Trans* 2011;52(5):1048–52.
- [50] Wu P, Huang Y, Kang L, Wu M, Wang Y. Multisource synergistic electrocatalytic oxidation effect of strongly coupled PdM (M = Sn, Pb)/N-doped graphene nanocomposite on small organic. *Molecules* 2015;5:1–9.
- [51] W. Wen, C. Li, W. Li, Y. Tian, Carbon-supported Pd–Cr electrocatalysts for the electrooxidation of formic acid that demonstrate high activity and stability, *109* (2013) 201–206.
- [52] Conway B, Tilak B. Interfacial processes involving electrocatalytic evolution and oxidation of H₂, and the role of chemisorbed H. *Electrochim Acta* 2002;47(22–23):3571–94.
- [53] Chekin F. Sol-gel synthesis of palladium nanoparticles supported on reduced graphene oxide: an active electrocatalyst for hydrogen evolution reaction. *Bull Mater Sci* 2015;38(4):887–93 .
- [54] Tian J, Wu W, Tang Z, Wu Y, Burns R, Tichnell B, Liu Z, Chen S. Oxygen reduction reaction and hydrogen evolution reaction catalyzed by Pd–Ru nanoparticles encapsulated in porous carbon nanosheets. *Catalysts* 2018;8:329. doi:10.3390/catal8080329.
- [55] Huang B, Chen L, Wang Y, Ouyang L, Ye J. Paragenesis of palladium-cobalt nanoparticle in nitrogen-rich carbon nanotubes as a bifunctional electrocatalyst for hydrogen-evolution reaction and oxygen-reduction reaction. *Chem Eur J* 2017;23:7710–18.
- [56] Ensafi AA, Atashbar NZ, Mohamadi Z, Abdolmaleki A, Rezaei B. Pt-Pd nanoparticles decorated sulfonated graphene-poly(3,4-ethylenedioxythiophene) nanocomposite. An efficient HER electrocatalyst. *Energy* 2017;126:88–96.
- [57] Safavi A, Kazemi SH, Kazemi H. Electrocatalytic behaviors of silver-palladium nanoalloys modified carbon ionic liquid electrode towards hydrogen evolution reaction. *Fuel* 2014;118:156–62.
- [58] Zhang Z, Han S, Wang C, J Li, Xu G. Single-walled carbon nanohorns for energy applications. *Nanomaterials* 2015;5:1732–55.
- [59] Tan X, Zhang J, Wu X, Wang Y, Li M, Shi Zujin. Palladium nanoparticles loaded on nitrogen and boron dual-doped single-wall carbon nanohorns with high electrocatalytic activity in the oxygen reduction reaction. *RSC Adv* 2018;8:33688–94.
- [60] Li Y, Murthy AA, DiStefano JG, Jung HJ, Hao S, Villa CJ, Wolverton C, Chen X, Dravid VP. MoS₂-capped CuxS nanocrystals: a new heterostructured geometry of transition metal dichalcogenides for broadband optoelectronics. *Mater Horiz* 2019. doi:10.1039/C8MH00809D.